J. Phys.: Condens. Matter **12** (2000) 2291–2296. Printed in the UK PII: S0953-8984(00)07127-7

Local interactions of ^{57}Fe after electron capture of ^{57}Co implanted in α-Al_2O_3 and in α-Fe_2O_3

I Dézsi†‖, I Szűcs†, Cs Fetzer†, H Pattyn‡, G Langouche‡, H D Pfannes§ and R Magalhães-Paniago§

† MTA-KFKI Research Institute for Particle and Nuclear Physics, H-1525 Budapest 114, PO Box 49, Hungary

‡ IKS, Katholieke Universiteit Leuven, B-3001 Leuven, Belgium

§ Departamento de Física, Universidade Federal de Minas Gerais, Belo Horizonte, Brazil

Received 20 August 1999, in final form 19 January 2000

Abstract. α-Al_2O_3 and α-Fe_2O_3 were implanted with ^{57}Co at room temperature. α-Al_2O_3 showed complex Mössbauer spectra indicating paramagnetic hyperfine splitting for high-spin Fe^{3+} and electric quadrupole-split spectra for Fe^{2+} ions. In canted antiferromagnet α-Fe_2O_3, the implanted Co atoms were positioned substitutionally in Fe_2O_3 and at higher doses in Fe_3O_4 and in $Fe_{1-x}O$. In the different phases, the ions were in Fe^{2+} and/or in Fe^{3+} states after the electron capture of ^{57}Co; no after-effects were observed. The results suggest that the phases are formed during fast cooling and crystallization of the oxide from the high-temperature state of the thermal spike.

1. Introduction

Early studies on insulators (mostly on oxide structures) showed [1, 2] that insulators are either amorphized or remain crystalline after ion bombardment depending on the crystalline temperature/melting point ratio. For α-Al_2O_3 and α-Fe_2O_3 it was found that they become amorphous after ion bombardment at intermediate or at high doses. Later these two oxides were studied in more detail. The lattice location study of implanted Pb in α-Al_2O_3 at low doses ($\sim 10^{14}$ atoms cm^{-2}) showed that 80% of the Pb atoms are in substitutional positions [3]. High-dose (1.2×10^{17} atoms cm^{-2}) iron implantation in α-Al_2O_3 produced Fe^0, Fe^{2+}, Fe^{3+} charge states [4]. The implanted samples remained crystalline and became amorphous only when the implantation was performed at low temperature (77 K) [5]. α-Fe_2O_3 implanted with ^{57}Fe was studied by Mössbauer effect above 2×10^{16} atoms cm^{-2} dose values and it was found that a large fraction of iron is in the Fe^{3+} charge state in the substitutional position. Also, two other phases Fe_3O_4 (magnetite) and FeO were observed. Their relative fractions depended on the doses, and the values were the same as those given in the equilibrium Fe–O phase diagram for the various iron concentrations in the implanted layer [6]. This result is surprising: it may suggest that the final state around the implanted atoms is very similar to what it is in quenched oxides.

In order to find out more about the local state and interactions of the implanted atoms in α-Al_2O_3 and in α-Fe_2O_3, we performed Mössbauer studies on ^{57}Fe formed after EC of ^{57}Co implanted at low doses. In contrast to the case for ^{57}Fe implanted probe atoms, in ^{57}Co source experiments the information on the interactions is obtained exclusively on the implanted atoms.

‖ Also at: KFKI Research Institute for Technical Physics and Materials Science, Budapest, Hungary.

0953-8984/00/102291+06$30.00

2. Experimental details

Spectral grade ceramic α-Al_2O_3 and α-Fe_2O_3 samples were implanted with ^{57}Co and with ^{59}Co (for higher dose values) at 80 keV in the Leuven isotope separator at room temperature. Polycrystalline samples were chosen because in this case correlation of the parameters presents fewer difficulties in the analysis of the spectra composed of several overlapping components. The Mössbauer spectra were measured by a conventional spectrometer in constant-acceleration mode at room temperature. For single-line absorber $Na_4[^{57}Fe(CN)]_6$ with ^{57}Fe, a thickness of 0.5 mg cm^{-2} was used. Analysis of the measured spectra was performed using a least-squares program. The isomer shifts (δ) are given relative to that of α-iron. For a better comparison of the δ-values of the sources to the values of stable iron oxide phases, the negative sign of the δ-value of the source experiments was changed to positive. In order to calculate the distribution of the implanted atoms, the TRIM code was used [7].

3. Results and discussion

Figure 1 shows the measured and fitted Mössbauer spectra for α-Al_2O_3. The resonance lines at higher velocity values indicate an Fe^{3+} paramagnetic hyperfine-split spectrum component. The paramagnetic hyperfine-split spectrum for Fe^{3+} has been simulated using the formalism for calculation presented in reference [8]. This method is based on a simplified *ab initio* model which is equivalent to the Clauser–Blume model [9]. A static spin Hamiltonian for Fe^{3+} ($S = 5/2$) with crystal-field parameters $B_4^0 = -100$ mm s^{-1}, $B_4^3 = 0.001$ mm s^{-1}, magnetic hyperfine interaction with $A_x = A_y = A_z = -2.61$ mm s^{-1} (ground state) and 1.49 mm s^{-1} (excited state), and quadrupole interaction parameter $P = 0.25$ mm s^{-1} and asymmetry parameter $\eta = 0$ was used. The (δ) value was 0.36 mm s^{-1}. Electronuclear eigenstates of the Hamiltonian were calculated, to represent the Liouville and relaxation superoperators. The relaxation matrix was built up assuming a first-order dynamical spin-Hamiltonian, white-noise approximation, and an expansion of the relaxation matrix up to second order in the dynamical spin-Hamiltonian parameters [9,10]. The reservoir correlation spectral densities different from zero were $I'_{11} = I'_{-1-1} = I''_{11} = I''_{-1-1} = \lambda$, where λ is proportional to the rate of the transition between levels $S_z = \pm 1/2 \leftrightarrow \pm 3/2 \leftrightarrow \pm 5/2$. The spectrum with an implantation dose of 5×10^{13} atoms cm^{-2} was simulated with $\lambda = 0.05$ mm s^{-1} and that with 2×10^{14} atoms cm^{-2} dose with $\lambda = 0.07$ mm s^{-1}. Both spectra were calculated at the angle of 55° between the γ- and z-directions near to the magic angle, in order to simulate the polycrystalline sample. In the simulations the temperature value was 300 K (nearly equal populations of Kramers doublets) and the linewidth used was 0.28 mm s^{-1}. The simulated intensities (shown as SIM in figure 1) were subtracted from the experimental spectra; after this, the remaining parts of the spectra were fitted by the least-squares method. The fitting resulted in two quadrupole doublets and one single-line component. In the spectrum of the sample implanted with the lower dose value, the single-line component can clearly be seen. The hyperfine interaction parameters obtained after fitting are shown in table 1.

The (δ) values of the doublets indicate the presence of Fe^{2+} in high spin states. The δ-value of the single line is in between the values characteristic of Fe^{2+} and Fe^{3+} ionic states; the intermediate δ-value may indicate an electronic state with an electron-density value similar to that of the state formed by electron hopping between Fe^{2+} and Fe^{3+} ions as was observed for magnetite [11].

α-Al_2O_3 and α-Fe_2O_3 have rhombohedral structure with space group D_{3d}^6. The metal ions are positioned in the trigonally distorted octahedra of O^{2-} ions. The hyperfine interaction parameters of Fe^{3+} suggest that the paramagnetic hyperfine-split component of ^{57}Fe in α-Al_2O_3

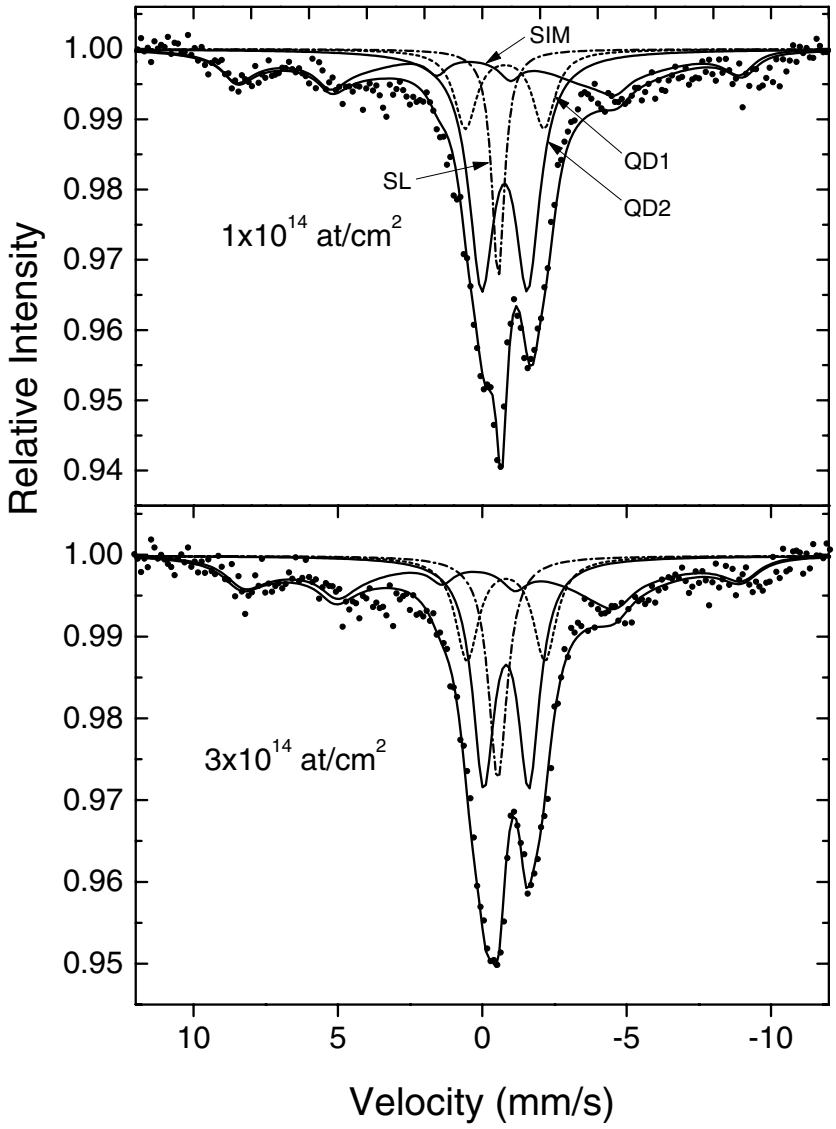

Figure 1. Mössbauer spectra of ^{57}Fe in α-Al_2O_3.

may be attributed to ions located in the octahedral lattice positions. The values of δ and ΔE_Q for the Fe^{2+} components agree with those measured for ^{57}Fe implanted in α-Al_2O_3 at low doses [12]. The presence of these components was related to that of the ones found in $FeAl_2O_4$ spinel. However, the values of ΔE_Q are significantly larger than those [13] characteristic of $FeAl_2O_4$ at room temperature. Because the average concentration of Co is rather low in the implanted volume, it is more probable that the implanted Co atoms decaying to Fe^{2+} are also located in the distorted octahedra in the Al_2O_3 lattice. The lower charge state of the ions is compensated by oxygen vacancies formed in the implantation process.

Figure 2 shows the spectra of α-Fe_2O_3. The spectra measured for α-Fe_2O_3 are quite different from that measured for α-Al_2O_3. At low dose values, the spectra show one magnetically

Table 1. Hyperfine interaction parameters of the implanted α-Al_2O_3 samples.

Component	δ (mm s^{-1})	ΔE_Q (mm s^{-1})	Γ (mm s^{-1})	Relative fraction (%)	Dose (atoms cm^{-2})
QD1	0.78(2)	2.72(2)	0.92(2)	13.8(5)	1×10^{14}
QD2	0.78(2)	1.59(2)	1.05(3)	44.7(5)	
SL	0.55(2)		0.52(2)	11.6(4)	
QD1	0.82(2)	2.70(2)	0.96(2)	17.4(5)	3×10^{14}
QD2	0.81(2)	1.57(2)	0.91(2)	34.8(4)	
SL	0.54(2)		0.77(4)	15.4(5)	

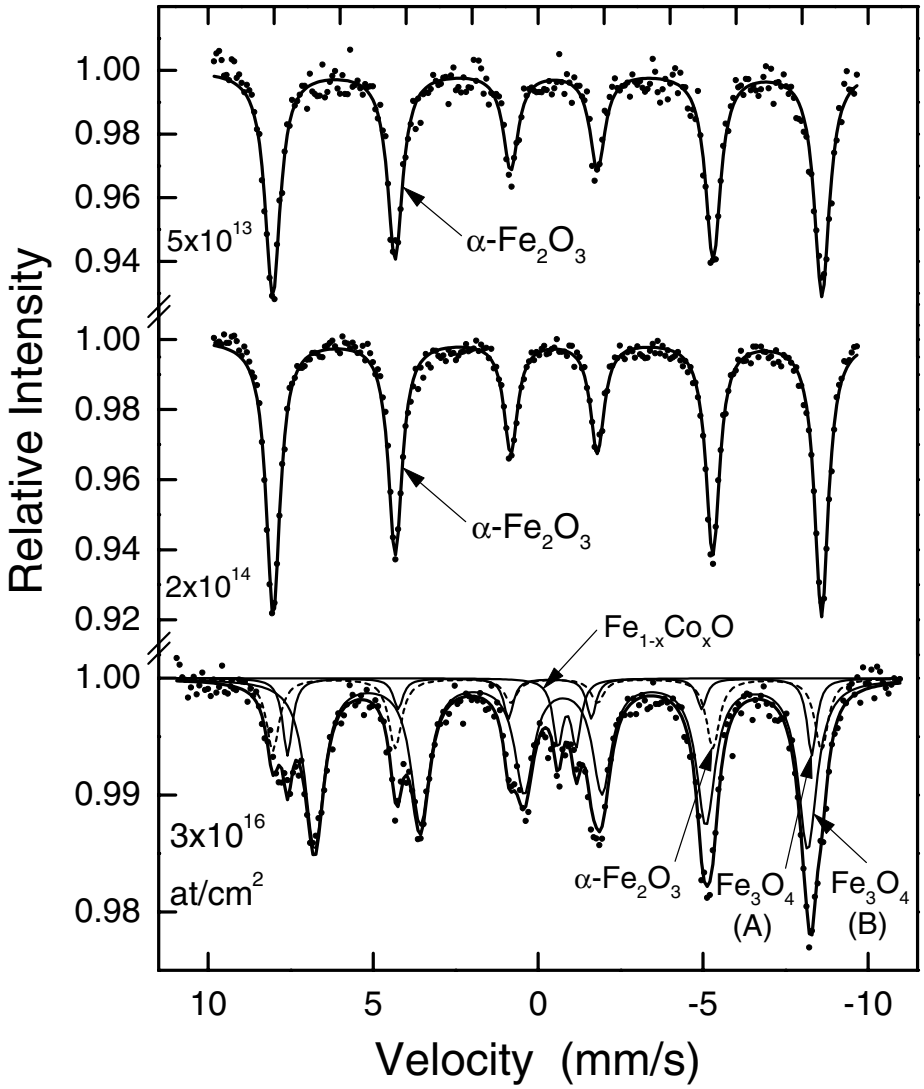

Figure 2. Mössbauer spectra of ^{57}Fe in α-Fe_2O_3.

split component with magnetic hyperfine interaction values equal to the value for ^{57}Fe in the pure target crystal [14]. Table 2 gives the hyperfine interaction parameters and the relative fractions of the components. The same quadrupole-splitting values for the implanted ^{57}Fe and for the pure α-Fe_2O_3 indicate that the angle of the spin direction to the c-axis in the implanted phase is also the same as in the pure α-Fe_2O_3 above the Morin transition.

Table 2. Hyperfine interaction parameters of the implanted α-Fe_2O_3 samples.

Phase	δ (mm s^{-1})	ΔE_Q (mm s^{-1})	HF (T)	Γ (mm s^{-1})	Relative fraction (%)	Dose (atoms cm^{-2})
α-Fe_2O_3	0.38(2)	0.20(2)	51.9(5)	0.58(2)	100	8×10^{13}
α-Fe_2O_3	0.39(2)	0.20(2)	51.5(5)	0.45(2)	100	2×10^{14}
α-Fe_2O_3	0.38(2)	0.20(2)	51.5(5)	0.47(2)	18(2)	3×10^{16}
Fe_3O_4–A	0.35(2)	0.01(5)	49.3(5)	0.35(2)	11(2)	
Fe_3O_4–B	0.73(2)	0.06(5)	46.3(5)	0.69(3)	66(5)	
$Fe_{1-x}O$	−0.88(2)	0.55(3)		0.35(3)	5(2)	

At an implanted dose of 3×10^{16} atoms cm^{-2}, the values of the hyperfine interaction parameters indicate that the implanted ^{57}Co is located in three phases: α-Fe_2O_3, Fe_3O_4 (magnetite), and cation-deficient [15] $Fe_{1-x}O$, the latter showing a quadrupole-split doublet. Since the ratio of the Mössbauer–Lamb factors of the A (tetrahedral) and B (octahedral) positions in the magnetite phase is 0.94(2) at room temperature [16], the ratio of the relative intensities of the spectral components of the A and B positions is 1:6 instead of close to 1:2—the latter in pure magnetite. This difference may indicate that the majority of the implanted Co ions are located at octahedral positions. This seems reasonable because Co prefers the 2+ to the 3+ ionic state and prefers to build into the B sites of the inverse spinel magnetite. At low dose values, the spectra of (^{57}Co)^{57}Fe appearing with the characteristic hyperfine interaction values of α-Fe_2O_3 indicate substitution for Fe with Co in α-Fe_2O_3. At the higher dose value, however, the average relative fraction of metals in the oxide increases from 40 to 42.8%. At around the maximum of the depth distribution, the relative concentration reaches 45%. In the phase diagram [17] of Fe–O, at these concentration values, the Fe_3O_4 and FeO phases are present. Formation of these stable phases may indicate that during implantation heat spikes are formed and the temperature value in the cascade volume is close to the non-congruent melting temperature of Fe_2O_3 (1855 K). On cooling down, crystallization occurs resulting in the different phases being present in a relative concentration corresponding to the metal/oxygen ratio in the implanted volume. The Co atoms are built into these phases.

There is now ample evidence showing that the high ion beam mixing efficiency cannot be understood in terms of ballistic two-body collisions but can be attributed to the formation of melting in displacement cascades [18]. Simulations by molecular dynamics calculation [19–23] have demonstrated that the model of surface melting provides a straightforward explanation for the formation of dislocation loops in implanted metals and for the formation of potholes on the surface of implanted silicon. The calculated temperatures in the implanted volumes extended to a few thousand K in these implanted materials. Because of the high energy loss per unit length for the implanted atom in the 50–100 keV energy region, the high temperatures in the collision cascades of transition metal oxides are highly probable. Ion-beam-induced creep in vitreous SiO_2 could be understood by supposing there to be thermal spikes even for this low-Z material [24]. The present experimental result on α-Fe_2O_3 indicates the existence of high temperatures in the displacement cascade zones.

4. Conclusions

The Mössbauer spectra of implanted ^{57}Co in α-Al_2O_3 after electron capture showed Fe^{2+} and Fe^{3+} ionic states, the latter with paramagnetic hyperfine splitting. The spectra of α-Fe_2O_3 are quite different from that measured for α-Al_2O_3. At low dose values, the spectra show one magnetically split component with magnetic hyperfine interaction values and electric quadrupole splitting equal to the values for ^{57}Fe in the pure target crystal, indicating the substitution for Fe with Co in the α-Fe_2O_3 lattice. At higher dose, the hyperfine interaction values indicate that the implanted ^{57}Co is located in three phases: α-Fe_2O_3, Fe_3O_4 (magnetite), and cation-deficient $Fe_{1-x}O$. From the formation of these stable phases, the formation of heat spikes can be concluded. On cooling down, crystallization occurs, resulting in the different phases being present in a relative concentration corresponding to the metal/oxygen ratio in the implanted volume.

Acknowledgments

The work was supported by Grant No T 14235 (OTKA) and under the cooperation agreement between OMFB and the Ministry of the Flemish Community (No B14/96).

References

[1] Naguib H M and Kelly R 1975 *Radiat. Eff.* **15** 1
[2] Kelly R 1981 *Nucl. Instrum. Methods* **182+183** 351
[3] Drigo A V, Lo Russo S, Mazzoldi P, Goode P D and Hartley N E W 1977 *Radiat. Eff.* **33** 161
[4] Donnet C, Jaffrezic H, Marest G, Moncoffre N and Tousset J 1990 *Nucl. Instrum. Methods* B **50** 410
[5] McHargue C J, Sklad P S, McCallum J C, White C W, Perez A and Marest G 1990 *Nucl. Instrum. Methods* B **46** 144
[6] Binczycka H, Fornal B, Marest G, Moncoffre N and Stanek 1991 *J. Radiat. Eff. Defects Solids* **116** 97
[7] Ziegler J F, Biersack J P and Littmark U 1985 *The Stopping and Ranges of Ions in Solids* (New York: Pergamon)
[8] Pfannes H-D and Magalhães-Paniago R 1994 *Hyperfine Interact.* **83** 79
[9] Clauser M J and Blume M 1971 *Phys. Rev.* B **3** 583
[10] Dattagupta S, Shenoy G K, Dunlap B D and Asch L 1977 *Phys. Rev.* B **16** 3893
[11] Kündig W and Hargrove R S 1969 *Solid State Commun.* **7** 223
[12] McHargue C J, Farlow C C, Sklad P S, White C W, Perez A, Kornilios N and Marest G 1987 *Nucl. Instrum. Methods* B **19+20** 813
[13] Dormann J L, Seqqat M, Fiorani D, Nogues M, Soubeyroux J L, Bhargava S C and Renaudin P 1990 *Hyperfine Interact.* **54** 503
[14] Greenwood N N and Gibb T C 1971 *Mössbauer Spectroscopy* (London: Chapman and Hall) p 240
[15] Greenwood N N and Gibb T C 1971 *Mössbauer Spectroscopy* (London: Chapman and Hall) p 248
[16] Sawatzky G A, van der Woude F and Morrish A H 1969 *Phys. Rev.* **183** 383
[17] Wriedt H A 1993 *Diagrams of Binary Iron Alloy* ed H Okamoto (Materials Park, OH: ASM International) p 280
[18] Trinkaus H 1997 *Mater. Sci. Forum* **248–349** 3
[19] Hsieh H, Diaz de la Rubia T and Averbach R S 1989 *Phys. Rev.* B **40** 9986
[20] Diaz de la Rubia T and Guinan M W 1991 *Phys. Rev. Lett.* **66** 2766
[21] Ghaly M and Averbach R S 1994 *Phys. Rev. Lett.* **72** 364
[22] Averbach R S and Ghaly M 1994 *J. Appl. Phys.* **76** 3908
[23] Caturla M-J, Diaz de la Rubia T, Marqués L A and Gilmer G H 1996 *Phys. Rev.* B **54** 16 683
[24] Trinkaus H 1995 *J. Nucl. Mater.* **223** 196